2025-02-09

Synthesis and characterization of aminofunctionalized chitosan-silica nanocomposite for the removal of Cu2+ from waste water

Onoka, Isaac

Springer International Publishing

https://doi.org/10.1007/s43939-025-00215-9

Discover Materials

Research

Synthesis and characterization of aminofunctionalized chitosan-silica nanocomposite for the removal of Cu^{2+} from waste water

Isaac Onoka[1] · **Askwar Hilonga**[2]

Received: 19 October 2024 / Accepted: 3 February 2025
Published online: 09 February 2025

Abstract
This study presents the synthesis and characterization of an aminofunctionalized chitosan-silica nanocomposite using the polymer melt intercalation technique. Chitosan, a biopolymer with inherent biocompatibility and antimicrobial properties, was functionalized with amino groups to enhance its reactivity and potential applications. Silica nanoparticles were incorporated as the reinforcing agent, providing improved thermal and mechanical stability. The polymer melt intercalation method facilitated uniform dispersion of silica within the chitosan matrix, overcoming common agglomeration challenges. The synthesized nanocomposite was thoroughly characterized using Fourier Transform Infrared Spectroscopy (FTIR) to confirm chemical modifications, Scanning Electron Microscopy (SEM) to observe morphological features. X-ray Diffraction (XRD) was used to evaluate structural integrity and dispersion of silica within the polymer matrix. The results demonstrated successful aminofunctionalization and homogeneous silica distribution, leading to a significant improvement in mechanical strength, thermal resistance, and biodegradability. These findings suggest that 0.5 mg of the aminofunctionalized chitosan-silica nanocomposites removed 98% of Cu^{2+} from contaminated water at an extended pH range of 4 to 6. In addition, the nanocomposite exhibited a significant increase in adsorption capacity at a sample dose ranging from 10 to 50 mg in 50 ml of the model solutions.

Keywords Nanocomposite · Homogenous · Intercalation · Chitosan · Polymer matrix

1 Introduction

Chemical industries have recently expanded due to rising demand for industrial products. This has increased the complexity of harmful effluents in the environment, especially in water bodies. Various industrial operations produce wastes containing heavy metals, which, when discharged into the water systems, cause severe threats to life because of their potential toxicity, even at very low concentrations. Furthermore, heavy metals are not biodegradable and tend to persist in living organisms, resulting in various forms of illnesses such as cancer, stomach ailments, intestinal distress, liver and kidney damage, and anaemia. One such metals is copper which is produced from industrial processes such as electroplating, tannineries, textile industries, copper mining and smelting, brass manufacture, petroleum refineries, electroplating and the disproportionate use of Cu-based agrochemicals and is potentially hazardous to humans [1].

The present physicochemical techniques for copper removal, such as precipitation, reduction, and ion exchange, are costly and inefficient in high amounts. They also produce metal-bearing sludge, which is difficult to dispose

✉ Isaac Onoka, onokaisaac@gmail.com; Askwar Hilonga, askwar.hilonga@nm-aist.ac.tz | [1]Department of Chemistry, University of Dodoma, Dodoma, Tanzania. [2]Department of Materials, Water and Environmental Science, Nelson Mandela Africa Institution of Science and Technology, Arusha, Tanzania.

of, adding more challenges to the industrial waste treatments. Biosorption using bioplastics has been a promising alternative solution to conventional processes.

Chitosan (Fig. 1b) is a derivative of chitin polysaccharides (Fig. 1a) consisting of varying amounts of β (1–4) linked residues of *N*-acetyl-2 amino-2-deoxy-D-glucose. It has a similar structure to chitin, but the difference between them is the deacetylation degree (DD) and their respective solubility in dilute acidic media [2]. For many years, chitosan has drawn the interest of many researchers due to its novel properties such as biocompatibility, nontoxicity, biodegradability, heat resistance, adsorption properties, stability in a pH range and so on [3, 4]. These qualities have made chitosan valuable in various applications, including film production, cell culture medium, optical material, and chelating agent [5–7].

Chitosan-metal interaction is an essential aspect of the adsorption capacity of chitosan. Chelation and electrostatic interaction are two modes described in most studies [8]. A pH close to neutral or in a non-protonated form, lone pairs in nitrogen can be used as donor atoms to form a coordinated bond with transition metals such as Cu^{2+}, Ni^{2+}, Zn^{2+}, etc., and at a low pH where protonation of the amine group occurs.

The biosorption properties of chitosan can be improved by introducing various materials in the polymer matrix of chitosan [9]. Multiple studies have been reported, and many more are underway. Recently, researchers have studied chitosan in various compositions and applications that include the preparation of chitosan/silica hybrids and chitosan-silica complex membranes [9, 10], little information in the literature has been found about applying a layered nanocomposite of chitosan and silica to remove heavy metals from water.

This study aimed to synthesize a homogenous chitosan-silica nanocomposite using an polymer melt intercalation technique. It was chosen for the synthesis of aminofunctionalized chitosan-silica nanocomposites due to its efficiency in achieving uniform dispersion of nanoparticles within the polymer matrix. Silica nanoparticles tend to agglomerate due to their high surface energy. The polymer melt intercalation method utilizes high shear forces and thermal energy to effectively exfoliate and distribute nanoparticles, ensuring homogeneity within the chitosan matrix. The method involves preparing a polycondesed silicate (played silicate), mixing the layered silicate with a polymer and then heating the mixture at a temperature above the softening point of the polymer. This method will improve the interaction between polymer functional groups and the silica nanoparticles by derivatizing the silicates with ethyl ammonium cations via an ion exchange reaction, consequently favouring the compatibility between chitosan and silica functional groups. The surface functionalization of the silica surface characteristics will form polymer-layered chitosan-silicate (PLS) nanocomposites that will exhibit properties different from the conventional chitosan silica composites.

It is anticipated through this study that the introduction of silica nanoparticles with derivatized surfaces into the chitosan polymer matrix will improve the properties of the chitosan towards water treatment and purification, increasing water permeation with maintained selectivity, improve structure by providing polymercrosslinking by introducing using functionalized silica. Introducing silica nanoparticles will create extra free volumes in the polymer matrix, increasing permeation. Furthermore, introducing silica into the chitosan matrix will not only prevent the dissolving of the polymer when metal sorption is performed in acidic media but also enhance the sorption capacity. Also, modifying the inorganic surfaces will improve compatibility between the two phases and strengthen the formation of a strong linkage between the organic and the inorganic phases via covalent bonds. A similar technique has been applied to produce polymer-layered silicate nanocomposites and a few commercial applications.

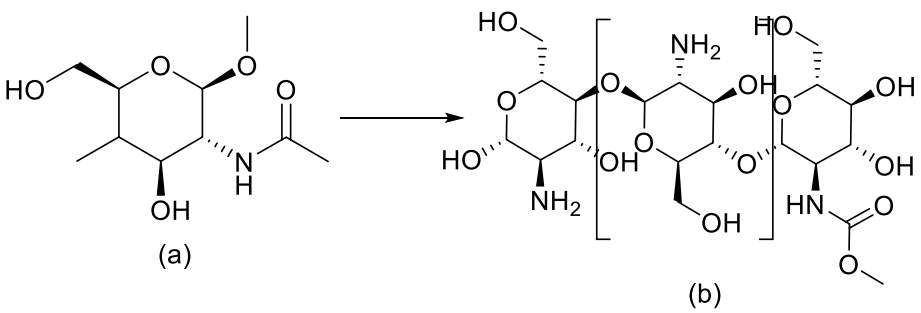

Fig. 1 Chemical structures of chitin and chitosan: **a** acylated chitin and **b** deacylated chitosan

2 Materials and methods

A low molecular weight chitosan (150–250 kDa) was obtained from Sigma Aldrich and was used for this study. Sodium silicate was used as a precursor and was procured from Shinwoo Materials Co. Ltd, South Korea. Ethyl alcohol was secured from Sigma Shinwoo and was used without further treatment. Other chemicals were obtained from Sigma Aldrich.

2.1 Synthesis of the nanocomposite

Intercalated chitosan-silica nanocomposite was prepared using a combined method, as stated elsewhere or in other sources [11–13]. 1.5% w/v of chitosan was dissolved in 2.5% weight acetic acid at temperature of 65 °C. The solution was stirred at 400 rpm for 5 h to ensure a uniform dissolution of chitosan in acetic acid; the solution was filtered, degassed and labelled CS. Using sodium silicate as a precursor for silica, silica solution was prepared through a method proposed by Jongwattanapisan 12. In brief, 40% v/v silica solution was dissolved in deionized water and then allowed to undergo condensed polymerization by activating with 0.1 M HCL and stirred for 1 h. Ethylammonium solution was prepared by bubbling ammonia through ethyl alcohol.

Different amounts of the polycondesed silica (100 cm^3, 70 cm^3 and 40 cm^3) were mixed with chitosan solution and ethyl ammonium solution in the ratio of 4:2:1, 4:1.5:1, 4:1:1 and were labelled CO1, CO2 and CO3 respectively. The hybrids were stirred for 24 h and then aged with 5 M H_2SO_4, followed by intercalation by heating the solution mixture above the chitosan softening point. The hybrid mix was then cooled, washed with distilled water until the pH was 7, and dried in a vacuum oven for 24 h.

2.2 Characterization of the nanocomposite

The XRD analysis was done to evaluate the crystallinity. The spectra were collected using an XRD machine (RIGAKU CORPORATION, D/MAX-2500/PC) with CuKα radiation at 40 kV and 100 mA. The 2θ scan range was 5–50° with a step size of 0.1° and a time/step of 1 s. Field Emission Scanning Electron Microscopy (SEM-Hitachi-s-4800, Japan) was used to study the surface morphology of the nanocomposite. An accelerating voltage of 15 kV was used to obtain the SEM micrographs. The SEM was coupled with energy dispersive spectroscopy (EDX) to analyze the sample's purity and elemental composition under analysis. The study of the Distribution of the particles in the synthesized nanocomposite was done using high-resolution transmission electron microscopy (HRTEM, Jeol JEM 2100F-Korea). The sample was dispersed in ethanol solution and then sonicated using ultrasonic bathing for 1 h to ensure uniform dispersion of the particles. The grid slides were immersed in the dispersed composite solution, and the solvent evaporated. For the FT-IR absorption measurements, the FT-IR Spectrometer (Avatar 360 E.S.P, Nicolet) was used to determine the bonding pattern of the synthesized nanocomposite mixture. The nanocomposite powder was mixed with KBr and pressed into pellets at 8 tons for 1 min. The pellets were analyzed at an average scan of 64 scans with wave number collected from 400 to 4000 cm^{-1} and optical velocity of 0.6334 cm^{-1}. To analyze the surface area and porosity of the sample, Brunauer–Emmett–Teller (BET) uses the nanocomposite's N2 adsorption–desorption instrument (Micrometrics ASAP 2020). All the samples examined were degassed at 200 °C for 2 h before actual measurements. Pore size distribution (PSD) and specific desorption pore volumes were obtained using the Barrett–Joyner–Halenda (BJH) method, and desorption branches were used to determine the PSD.

The prepared chitosan-silica nanocomposite was tested to remove heavy metals from the aqueous solution. $CuSO_4 \cdot 5H_2O$ was used for this study through a similar method(s) [14]. 10 ppm of copper was prepared by dissolving 0.392 g of $CuSO_4 \cdot 5H_2O$ in 1 l of distilled water and then stirred with a magnetic stirrer for 5 h at 25 °C. The resulting solution was used as a standard stock copper solution for the succeeding experiments. Inductively Coupled Plasma Atomic Absorption Spectroscopy (ICP-AAS) determined the initial and final concentration of copper.

The adsorption amount was calculated by the equation.

$$Q = \frac{(C_o - C)V}{m} \tag{1}$$

where *Q* is the absorption capacity in (mg/g), C_o is the initial concentration, C is the final concentration, *V* is the volume of the solution in (L), and *m* is the weight of the nanocomposite in (g).

2.3 Adsorption properties of the nanocomposite

2.3.1 Effect of the nanocomposite doze

The effect of the nanocomposite doze of CO1, CO2 and CO3 on the adsorption of copper was investigated. Various amounts of the nanocomposites (0.01–0.05 g) were dissolved in 50 ml of $CuSO_4 \cdot 5H_2O$ containing 10 ppm of Cu^{2+}, stirred for 5 h and then filtered to determine the copper concentration remaining in the solution. The initial and the final concentrations of copper were determined using an ICP-AAS, and the adsorption capacity was calculated using Eq. 1.

2.3.2 Effect of pH on copper retention

The effect of the pH on the adsorption of copper ions on the nanocomposite was investigated using a similar method by Chen et al. [15]. 0.5 g of the nanocomposite was dispensed in 200 ml of $CuSO_4 \cdot 5H_2O$ with 10 ppm of Cu^{+} and then stirred for 5 h at 25 °C. The pH of the solution was adjusted to 3, 4, 5, 6 and 7, the initial and the final concentration of copper was measured, and the adsorption capacity with respect to the pH of the model solution was calculated using Eq. 1.

2.3.3 Kinetics of adsorption

The chitosan-silica nanocomposite prepared at different silica concentrations was studied to investigate the Kinetics of adsorption of the nanocomposite. 0.8 g of the chitosan-silica nanocomposite was added in 400 ml of 10 ppm $CuSO_4.5H_2O$ solution at pH 5 [15] while stirring at room temperature. Then, 50 ml of the aliquots of the solutions at intervals of 1 h were filtered, and their concentrations of Cu^{2+} were measured using ICP-AAS. Finally, the adsorption capacity (Q) was calculated.

3 Results and discussion

3.1 Synthesis and characterization of the nanocomposite

An effective and efficient nanocomposite for retaining Cu^{2+} from water has been made. It consists of polycondesed silica nanoparticles embedded in chitosan polymer matrix with functional groups capable of interacting with heavy metal ions from contaminated water. Four stages, hydrolysis, poly-condensation, derivatization and crosslinking of the polymer matrix, were considered to clarify the reaction mechanism. Condensation was done by acid activation and water through a reaction shown below. The precursor sodium silicate is hydrolyzed in acid to form silanol, as shown in reaction (I). Silanol groups are polycondesed to form an inorganic glass-type material with hydroxyl groups on the surface (reaction II).

The interaction between the polycondesed silica and ethyl ammonium results in the formation of derivatized polysilicate (reaction (III)) in which further chitosan is mediated by the hydrogen bonds between silanol group and the oxy and amide groups of the chitosan molecule and also the covalent bond formed as a result of the esterification of the chitosan hydroxyl group and the silanol groups of the silica. This interaction results in an organic–inorganic nanocomposite hybrid with OH-groups and NH_2 groups capable of attracting heavy metals from contaminated water. The hypothetical structure (Fig. 2) shows functional groups contributed by chitosan and the polycondensed derivatized silicate.

Previous studies have maintained that the intercalation method involves an exchange of the metal cations that could be located between the crystal layers by organic cations such as alkylammonium cation [16]. The bonding interactions between chitosan functional groups and silica nanoparticles play a critical role in the structural stability of the chitosan-silica nanocomposite. These interactions ensure a robust and uniform distribution of silica within the chitosan matrix, which enhances mechanical, thermal, and chemical stability. Structurally, chitosan contains abundant hydroxyl (–OH) and amino ($–NH_2$) groups that can form hydrogen bonds with the silanol groups (–Si–OH) on the silica nanoparticles. The hydrogen bonding creates strong intermolecular forces, ensuring good adhesion between chitosan and silica. It can also help to maintain the dispersion of silica nanoparticles within the polymer matrix, reducing particle aggregation thereby enhancing the mechanical stability of the composite by forming a cohesive network. At certain low pH levels,

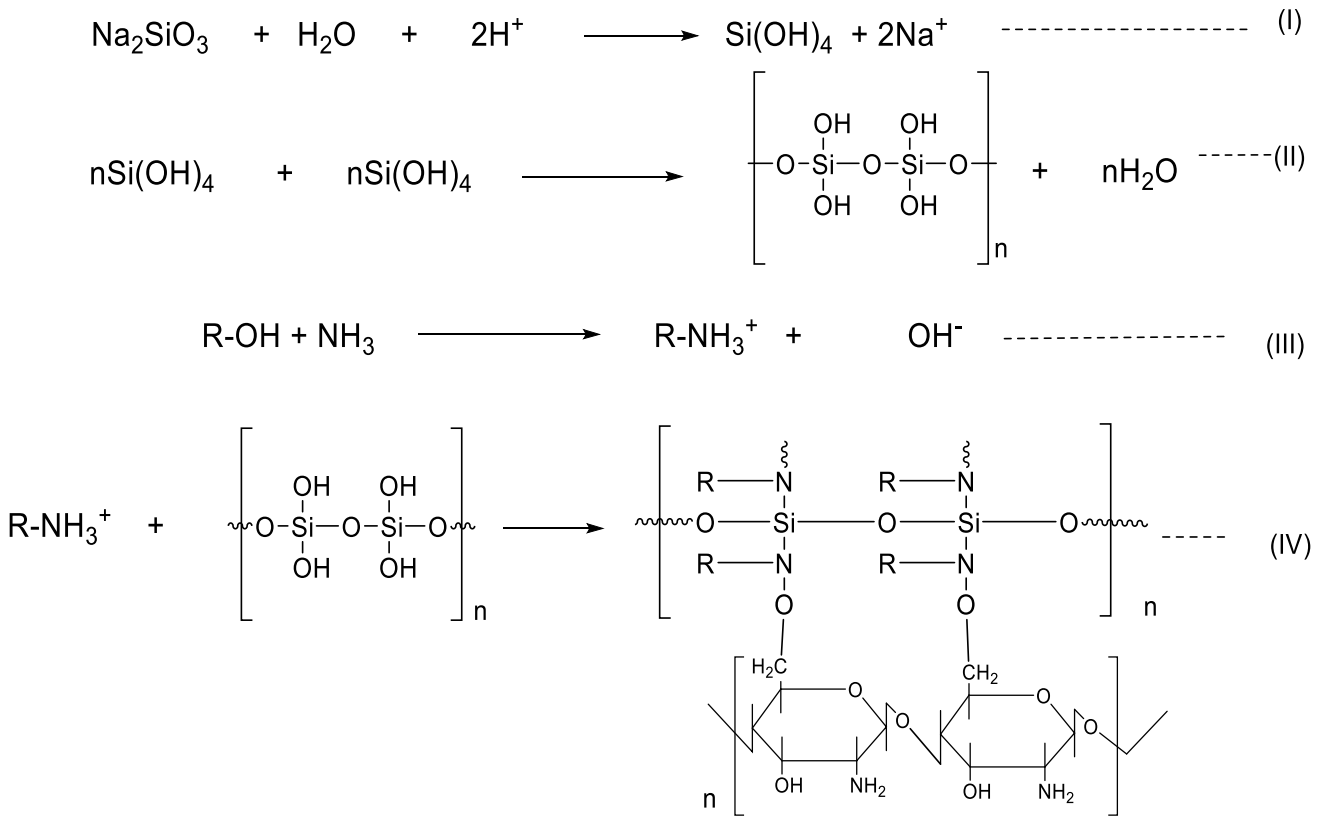

Fig. 2 Hypothetical structure of the chitosan-silica nanocomposite derivative with ethylammonium solution

chitosan can be protonated (forming -NH_3^+ groups), which interact electrostatically with negatively charged silica nanoparticles (from deprotonated silanol groups, –SiO^-). Electrostatic interactions strengthen the interface between chitosan and silica, especially in acidic conditions where chitosan is highly protonated help form a uniform distribution of silica, preventing phase separation.

Using ethyl ammonium cations lowered the surface energy of the inorganic particles and improved the polymer's wetting characteristic. As reaction IV shows, ethyl ammonium introduces additional functional groups into the polymer matrix. This allows a chemical reaction with the chitosan polymer and enhances the bonding between the functional and inorganic groups. Functionalizing silica with amine, thiol, or carboxyl groups have the potential to improve compatibility and bonding strength with chitosan [17].

3.2 Crystallinity

The XRD spectrum of the nanocomposite expresses a low-intensity expressive compared to pure chitosan, as indicated by Fig. 3c. The pattern exhibit broad, diffuse braggs peaks (also called halos) centred on 23°, indicating an amorphous structure of the nanocomposite. The absence of sharp diffraction peaks indicates that there is no long-range periodicity in the atomic arrangement of the material. Pure chitosan expresses characteristic peaks for non-crystalline, hydrated crystalline and anhydrous crystalline forms at around 10.02°, 14.34°, and 20.01°, which are in good agreement with the results of the previous study [18]. The crystallinity of the nanocomposite is typically low because silica is amorphous by nature and dominates the structure. Any crystalline domains from chitosan are diminished due to the high silica content disrupting its order. At a high chitosan content (low silica content) the crystallinity increases due to the greater presence of chitosan, which has semi-crystalline regions. The non-crystalline, hydrated crystalline disappears in the nanocomposite, followed by a shifting of the anhydrous crystalline peak to around 22.83°. The disappearance of these two crystalline peaks in the hybrid composite indicates the prominence of the chitosan amorphous structure, directly influencing the hybrid composite structure [19]. Furthermore, the shifting of the anhydrous crystalline peak from 20 to 22.02 was accompanied by the broadening of the 2θ. These observations provide clear evidence of the formation of the composite. It is evident through this study that the disappearance of the non-crystalline and the hydrated crystalline

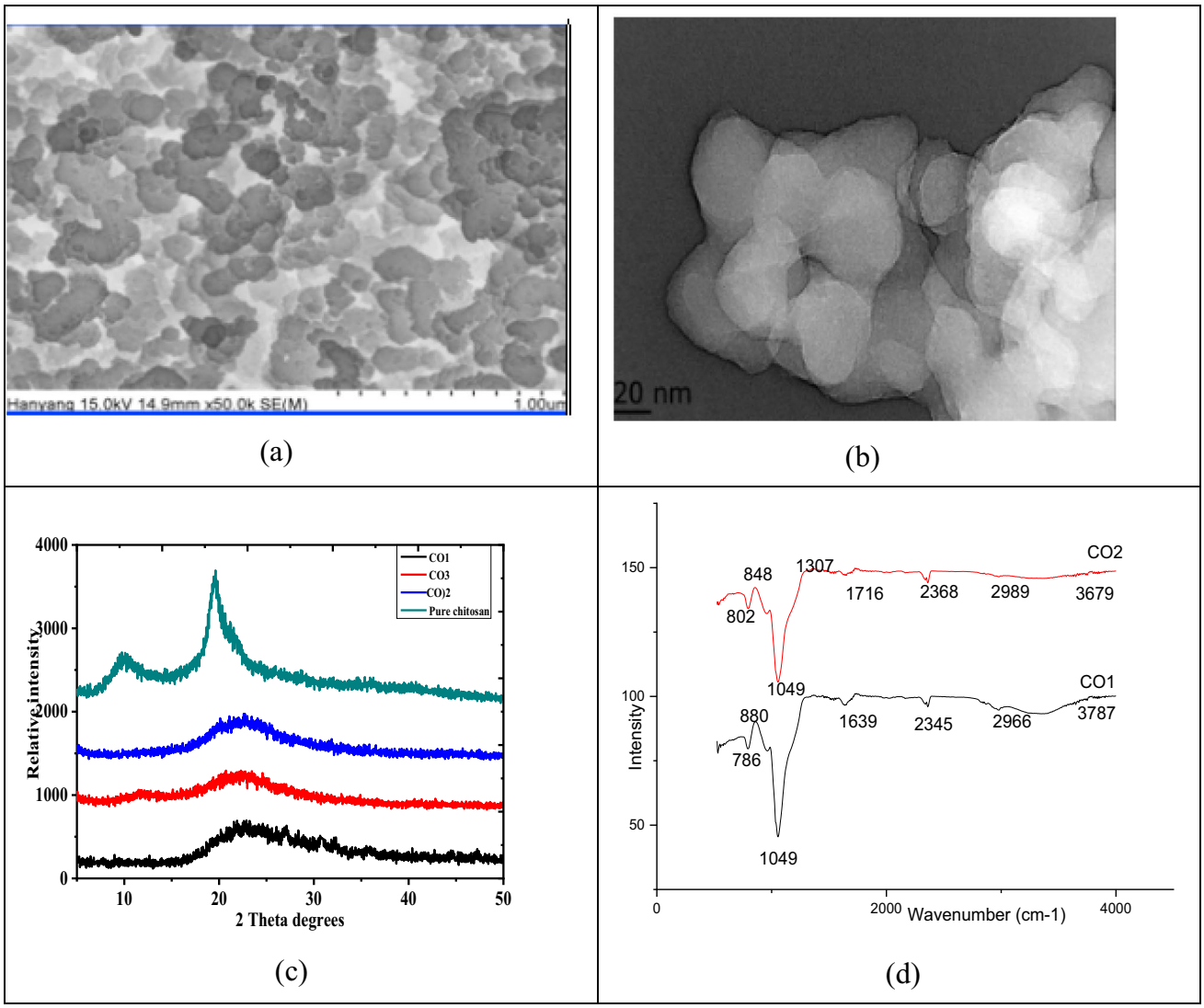

Fig. 3 SEM micrographs of (2a) CO1, (2b) CO2 and (2c) CO3. The silica nanoparticles are homogenously distributed into the chitosan polymer matrix. FE-TEM micrographs of CO1 (**a**, **c**), and CO3 (**b**, **d**) at different magnifications. CO1 has 25%v/v of silica, and CO3 has 11% v/v of silica. FT-IR spectrum of CO1 and CO2. XRD spectra (RIGAKU JAPAN) of a pure chitosan and chitosan-silica nanocomposite at different silica ratios prepared by intercalation

peaks is a function of the amount of silica contained in the hybrid. CO3 contains 16% silica (40% v/v), and a small non-crystalline peak can be seen; the peaks disappear progressively from CO2 (25%) to CO1 (33%).

3.3 Morphological and bonding pattern studies

The chitosan-to-silica ratio in a nanocomposite has a significant impact on its morphology and crystallinity due to the interaction between the organic (chitosan) and inorganic (silica) components. In principle, at low chitosan-to-silica ratio silica dominates the composition, leading to highly interconnected or aggregated silica particles. The surface may appear rough, with silica particles forming dense networks or clusters. Limited chitosan content results in less coverage of silica surfaces, exposing the rigid silica network. However in a high chitosan-to-silica ratio, chitosan becomes the dominant phase, leading to smoother surfaces due to the polymer encapsulating or dispersing the silica particles. The silica particles may appear more dispersed within the chitosan matrix, reducing particle aggregation. Excess chitosan can lead to the formation of polymer-dominated morphologies, such as films or coatings. The surface analysis of the nanocomposite has been effectively done using the SEM, and the results are represented in Fig. 3a. It was expected that the significant difference in the polymer properties and the silica nanoparticles could have resulted in a clear phase

separation. However, the SEM micrographs show no clear phase separation than the presence of microvoids. The SEM micrographs show spherical silica nanoparticles that are homogeneously dispersed in the chitosan polymer matrix, with the amount of the silica nanoparticles increasing with the increase of silica concentration. This feature indicates the formation of a nanocomposite of chitosan and silica. It agrees with the previously published results for composites of the two [7]. The particles were in the range of 20 nm as calculated using TEM micrographs Fig. 3b. With these results; the chitosan-silica complex membranes could be considered as nanocomposites consisting of homogeneously dispersed, nanosized inorganic silica reinforcements.

3.4 Distribution of the particles and layering of the nanocomposite

The effect of intercalation on the distribution of the particles inside the chitosan-silica nanocomposite was studied using HRTEM, and the results are represented by Fig. 3b. The silica nanoparticles are spherical and are embedded in a chitosan structure which acts as the polymer matrix. Figure 3a and b show the density of silica particles increases with the increase in silica concentration. It is evident that the silica particles are embedded in the chitosan polymer matrix, and the particles can be distinguished from the surface of the composite.

Intercalation at this synthesis temperature generated a porous nanocomposite with spherical and amorphous particles that are homogenously distributed; the results are in good agreement with the SEM images and the XRD analysis. The composite exhibited highly homogenous particles, with the silica particles silica showing no evidence of aggregation or monodispersion but rather existing in a polycondesed form Fig. 3b. This is clear evidence of the formation of polycondesed silica chains.

3.5 Bonding pattern

FT-IR spectra of the nanocomposite (Fig. 3d) show an absorption band between 500 cm^{-1} and 4000 cm^{-1}. A fully deacetylated chitosan has absorption bands that are characteristics of the prominent significant absorption bands of the stretching, bending and rocking vibration of N–H, O–H, C–H, C–N and C–O [20]. The band at 2966 cm^{-1} (CO1) and 2989 cm^{-1} (CO2) are assigned to C–H stretching vibration. These bands were expected to be at 2998 cm for a fully deacetylated chitosan [21]. The bands 3679 and 3787 cm^{-1} are associated with the stretching absorption band for N–H and O–H. For pure chitosan, these bands would have been observed at 3489 cm^{-1} [20]. N–H bending vibration is observed at the absorption band at 1716 cm^{-1} (CO2) and 1639 cm^{-1}(CO1), while the C–H bending is at 1307 cm^{-1}. The C–H and N–H bending vibrations are attributable to the absorption bands at 1049 cm^{-1} in both CO1 and CO2, different from the results from the previous study that reported 1041 cm^{-1} for pure chitosan [21, 22].

The formation of a chitosan-silica nanocomposite is demonstrated by a decrease in the absorption intensity of N–H functional groups and the emergence of new peaks associated with Si–OH, Si–O–R band [19]. This study demonstrates clear evidence for the formation of the nanocomposite by a decrease in intensity at the N–H absorption band at 1049 cm^{-1}. The intensity has been lowered to 46 in CO1 and 54 in CO2. The results further demonstrate that the decrease is intensified as the amount of silica increases in the sample, i.e. (CO1). The bands for Silanol (Si–OH) introduced into the polymer structures are observed at 991 cm^{-1} in CO1 and 983 cm^{-1} in CO2. These bands are not featured in the IR spectra of pure chitosan. They can be used as a distinguishing characteristic for forming a chitosan-silica composite, as suggested by Silva and his coworkers [19].

Another significant bonding feature is the sharpness of the absorption band between 1000 and 1100 cm^{-1}. This region is associated with the absorption band of Si–O–Si, with the sharpness increasing as the concentration of silica increases. Interestingly, the stretching vibrations of the –OH group are observed at the absorption bands between 3500 and 3700 cm^{-1}. The peaks are less sharp, indicating the formation of a strong bond. The bands' peaks between 700 and 900 cm^{-1} are associated with Si–O–Si axial deformation and Si–O–Si angular deformation [19].

3.6 The study of adsorption properties of the nanocomposite

3.6.1 Optimization of the nanocomposite and effect of the sample doze

The nanocomposite was optimized for the adsorption of Cu^{2+} by controlling the chitosan silica ratio. To a fixed volume of chitosan solution (1.5%w/v), different volumes of silica were added, hydrolyzed, polycondesed, and intercalated using ethylammonium solution. Figure 4a–c show the results for the adsorption of Cu^{2+} using CO1, CO2 and

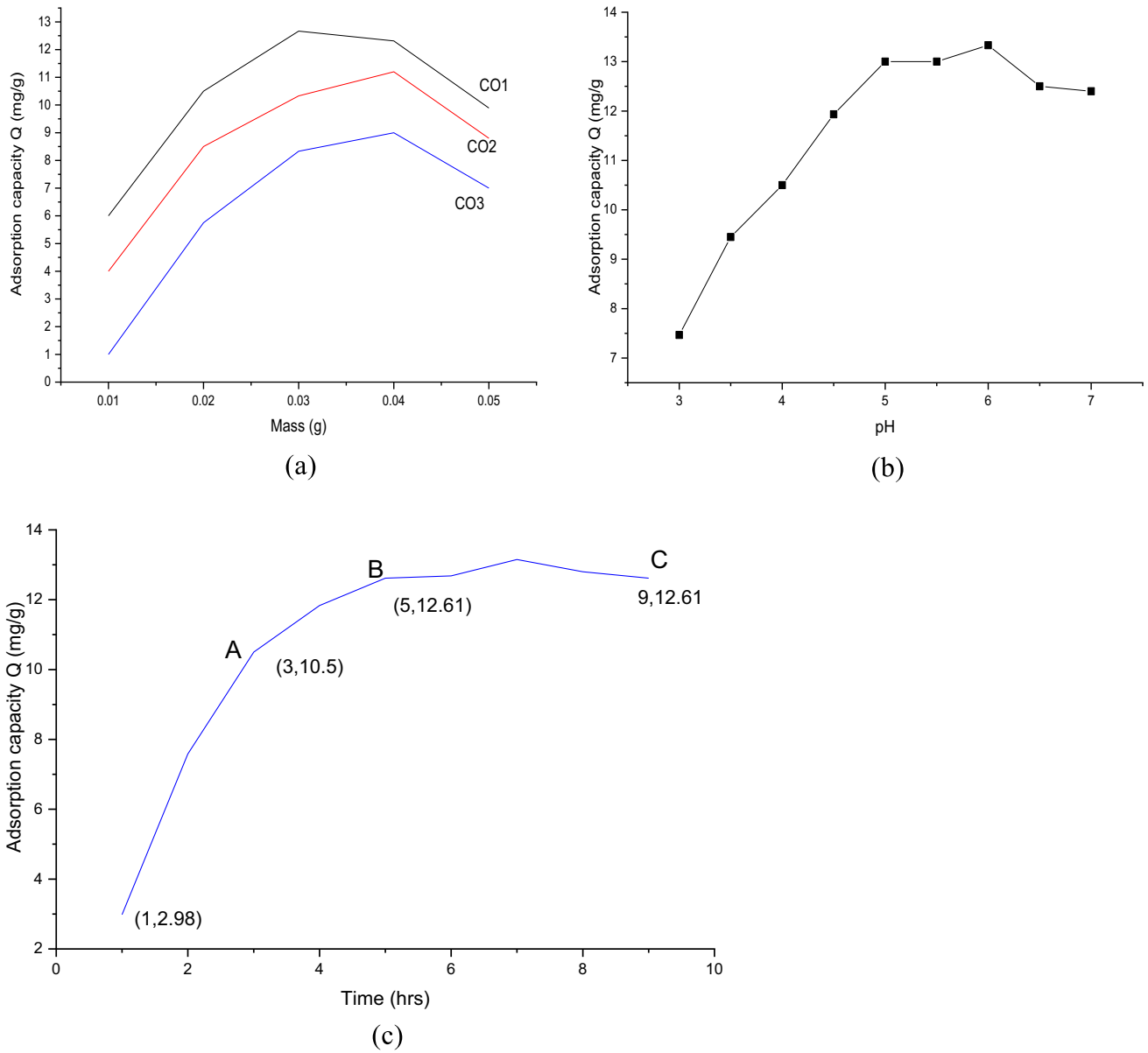

Fig. 4 Optimization of the nanocomposite and Effect of sample doze in the absorption of Cu^{2+} using different ratios of silica in chitosan., Effect of pH on adsorption of copper using 0.03 g 0f CO1 at 25 °C at an initial concentration of 10 mg/L, Effect of the contact time on the adsorption of Cu^{2+}

CO3. The nanocomposites show different adsorption capacities depending on the amount of silica contained in the sample. Generally, the adsorption capacity increases with the amount of silica contained in the chitosan polymer matrix. CO1, with the highest silica ratio, has a maximum adsorption capacity of 12.66 mg/g, followed by CO2. The three nanocomposites show a similar pattern in the adsorption of Cu^{2+}, similar to the results of the previous studies doneby Tumin and his coworkers [23].

As in Fig. 2, the nanocomposite is composed of functional –OH and $–NH_2$ groups responsible for the attachment of the heavy metals from contaminated water. The number of functional groups depends on the degree of deacetylation (DD) of the chitosan and the hybrid counterpart polycondensed silica and sample doze. This directly impacts the functional group loading capacity of heavy metal contaminants. Apparently, the amount of Cu^{2+} adsorbed on the composite increases with the increase in the composite doze. In this experiment, the effect of the nanocomposite doze on the adsorption of Cu^{2+} was investigated by varying the amount of the nanocomposite (0.01–0.05 g) in 10 ppm

of $CuSO_4.5H_2O$. The results demonstrate clearly that the adsorption capacity Q of the nanocomposites increases with increasing sample doze to an optimum sample doze, as supported by Fickian's equation for diffusion Eq. 2.

However, the adsorption density, the amount of Cu^{2+} adsorbed per unit mass, decreases with the increase in the nanocomposite doze after an optimum dose. At lower sample doze, the nanocomposite's Cu^{2+} adsorbed per unit mass is a high increase. Previous studies have made it evident that the number of active sites available for the adsorption of Cu^{2+} increases with the adsorbent dose. It is readily understandable that as the adsorbent dose increases, there is the emergence of intraparticle interaction, such as aggregation, that consequently results in a decrease in the total surface area of the adsorbent, increased diffusional path length and hence a decreased adsorption density [24]. This can be why the adsorption capacity is slightly decreasing at larger adsorbent doses.

3.6.2 Effect of the pH on copper retention

The effect of the pH on the adsorption of copper ions onto the nanocomposite was investigated using a similar method by Cheng et al. [15]. An optimum dose of the nanocomposite (0.03 g) was dispensed in 50 ml of $CuSO_4 \cdot 5H_2O$ with 10 ppm of Cu^+ and then stirred for 5 h at 25 °C. The pH of the solution was adjusted from 3 to 7, the initial and the final concentration of copper were measured, and the adsorption capacity with respect to the pH of the model solution was calculated using equation (I).The interaction of the nanocomposite functional groups and heavy metals is a function of the pH of the medium to which the adsorbent is subjected. The adsorption of Cu^{2+} as a function of pH increases with increasing pH similar to previous studies [25, 26]. The uptake of Cu^{2+} is attributed to the competitive adsorption of the proton and the metal cation via the coordination with the $–NH_2$ and the –OH groups present on the nanocomposite through reactions (I) and (II).

$$M^{2+} + nRNH_2 \longrightarrow M(RNH_2)^{2+} \quad \text{(I)}$$

$$H^+ + RNH_2 \longrightarrow RNH_3^+ \quad \text{(II)}$$

At higher pH, reaction (II) is more favoured than reaction (I), meaning that at higher pH, more Cu2 + are adsorbed onto the nanocomposite compared to the limited protonation from the H^+. Previous studies have shown similar results on the interaction of chitosan with heavy metals [20].

At a high pH the adsorption of Cu^{2+} at is described reactions (III and IV).

$$RNH_2 + OH^- \longrightarrow NH_2OH^- \quad \text{(III)}$$

$$RNH_2OH^- + Cu_2^+ \text{ (or } CuOH^+) \longrightarrow RNH_2OH^{\cdots} \cdot Cu_2^+ \text{(or } NH_2OH^{\cdot} \cdot CuOH^+) \quad \text{(IV)}$$

The protonation and the formation of the surface metal complex were regarded as reversible reactions (reaction I, II) [20]; however, a slightly different mechanism was described by ref. [27] considering the reaction (II) a protonation and deprotonation reaction while the formation of a surface metal complex between the $–NH_2$ and the Cu^{2+} to be irreversible.

It is likely that the introduction of the silica nanoparticles into the chitosan polymer matrix will increase –OH groups will be available for interaction with metal cations. This is evident from the increase in the nanocomposite's adsorption capacity compared to the pure chitosan proposed by ref. [20].

The zeta potential of both the chitosan and the silica nanoparticles can also explain the increase in the adsorption capacity of the nanocomposite. Thus, at a pH < 6.7, the electrostatic interaction between the chitosan functional groups and the Cu^{2+} becomes more repulsive, lowering the adsorption capacity, but a pH > 6.7 results in attractive electrostatic interaction between the metal ion and chitosan functional, which results to the increase in adsorption capacity.

The decrease in the adsorption capacity at the pH above 6.5 is further explained by the presence of competing groups for the adsorption on the functional groups of the adsorbent. As suggested by Tumin [23], three species, Cu^{2+}, $Cu(OH)^+$ and $Cu(OH)_2$, are present in the solution and are competing for the adsorption on the surface of the adsorbent. The former is in small quantities, while the latter is in large quantities, resulting in the nanocomposite's adsorption capacity to Cu^{2+}.

3.6.3 Effect of anions on the adsorption capacity of Coppers

The presence of anions in the model solution affects the adsorption of metal ions from a solution. It has been shown in this study that CO1 shows different adsorption capacities of Cu^{2+} when SO_4^{-2} and NO_3^- are present in the solution. At

pH 5.64, more Cu^{2+} are adsorbed when SO_4^{-2} are present in the solution than NO_3^-. A similar effect had been reported by Chen and his team in their comparison of the Effect of Cl^- and SO_4^{-2} on the adsorption of different metal cations [15]. This study maintained that the high adsorption of copper in the presence of SO_4^{-2} is attributable to the effective charge compensation and ionic binding in SO_4^{-2} compared to the low charge in NO_3^-.

Using chitosan-silica nanocomposites for heavy metal adsorption is promising, but their effectiveness for metals other than copper may face limitations due to differences in binding mechanisms, selectivity, and structural compatibility. Chitosan's amino (-NH_2) and hydroxyl (-OH) groups exhibit strong chelation with copper ions (Cu^{2+}), but their affinity for other heavy metals like lead (Pb^{2+}), mercury (Hg^{2+}), cadmium (Cd^{2+}), and chromium (Cr^{6+}) may be lower. Metals with different ionic radii, coordination numbers, or binding preferences may not interact as efficiently with the chitosan matrix. The adsorption of some metals is highly pH-dependent. For example: Chromium (Cr^{6+}) prefers acidic pH (due to electrostatic interactions with -NH_3^+ groups). Lead (Pb^{2+}) adsorbs better in neutral to alkaline conditions [8]. The nanocomposite may not perform well if the target metal requires a pH outside its optimal range for adsorption. Furthermore, in complex water matrices, other ions (e.g., Ca^{2+}, Mg^{2+}, Na^+) can compete with heavy metals for adsorption sites, reducing the nanocomposite's selectivity and capacity.

3.6.4 Adsorption kinetics

3.6.4.1 Effect of the contact time The uptake of Cu^{2+} on the nanocomposite is greatly influenced by the contact time between the Cu^{2+} and the functional groups of the adsorbent. The experimental result for this investigation is represented in Fig. 4c. It is evident through this study that the rate of adsorption of Cu^{2+} increases depending on the length of contact time between the adsorbent and the adsorbate.

The adsorption behaviour of the Cu^{2+} can be divided into regions A, B and C, as shown in Fig. 4. "A" the rate of adsorption of Cu^{2+} in region A is 3.75 mg/g/h, B records 1.055 mg/g/h, while region C has a constant rate of adsorption. The mechanism for the adsorption of Cu^{2+} can be explained in terms of theoretical models, bulk diffusion, film diffusion [28], intraparticle diffusion and finally, the chemical reaction [29] between the Cu^{2+} and the active sites of the composite. Since the stirring speed was < 400 rpm, it is logical to consider the bulk diffusion as a limiting factor.

The factor for the adsorption of Cu^{2+}.For this reason, the Fickian law of diffusion can be used to describe the effect of contact time on the adsorption of the Cu^{2+} as represented in Eq. 2 [30]

$$Q_t = 2C_o S\frac{\sqrt{Dt}}{\pi} \tag{2}$$

$$= k_d\, t^{0.5} \tag{3}$$

Q_t is the amount of Cu^{2+} adsorbed per unit weight per unit time in mg/g/sec, C_o is the initial concentration of Cu^{2+}, t is the time, D is the diffusion coefficient, and S is the specific surface area. Region A indicates that the adsorption rate is linear, meaning that the adsorption of Cu^{2+} on the surface of the composite increases with the length of the contact time. A decrease in the adsorption rate at region B is explained by the limiting factor of the initially attached Cu^{2+} onto the active sites of the composite. The incoming Cu^{2+} will have to wonder in the bulk solution, searching for the available active sites of nanocomposites for attachment, consequently lowering the adsorption rate. A decrease in the adsorption rate at region B evidences this. No reaction characterizes region C. It can be explained in terms of the saturation of the nanocomposite sites that no more site is available for the attachment of the Cu^{2+}, or the entire available Cu^{2+} has been used up in the reaction. To support this argument, an attempt was made to analyze the equilibrium concentration at region C; the residue was treated with a fresh solution of Cu^{2+}, and it was found that more Cu^{2+} was removed. This led us to conclude that all the available Cu^{2+} were used up in the reaction at region C, and there was no more available Cu^{2+}.

3.6.4.2 Sorption kinetics The adsorption kinetics of the nanocomposite was studied by using the most popular adsorption isotherms models namely Langmuir [27, 28, 31] and Freundlich [15] in accordance with experimental data. The experimental data was fitted into the model equations in order to understand the equilibrium behavior of Cu^{2+} onto the surface of the nanocomposite. Basically, the Langmuir isotherm model describes the adsorption of molecules onto a surface and is used primarily in surface chemistry. It assumes that adsorption occurs on a surface with a fixed number of adsorption sites, and each site can hold only one molecule (monolayer adsorption). It also assumes a uniform surface in which all adsorption sites are identical and equivalent, implying that the energy for adsorption at all sites is the same and at the same time the

adsorbed molecules do not interact with each other [28]. The Langmuir adsorption isotherm is given by the following equation Eq. (4):

$$\frac{q_e}{q_m} = \frac{K_L C_e}{1 + K_L C_e} \tag{4}$$

where: q_e = amount of adsorbate adsorbed per unit mass of adsorbent at equilibrium (mol/g), q_m = maximum adsorption capacity (mol/g), the maximum amount of adsorbate that can be adsorbed at the surface (when the surface is completely covered by adsorbate), C_e = concentration of adsorbate at equilibrium (mol/L) and K_L = Langmuir constant, related to the adsorption capacity and energy of adsorption. The Langmuir equation can also be written as shown in Eq. (5):

$$\frac{1}{q_e} = \frac{1}{q_m C_e} + \frac{1}{q_m} \tag{5}$$

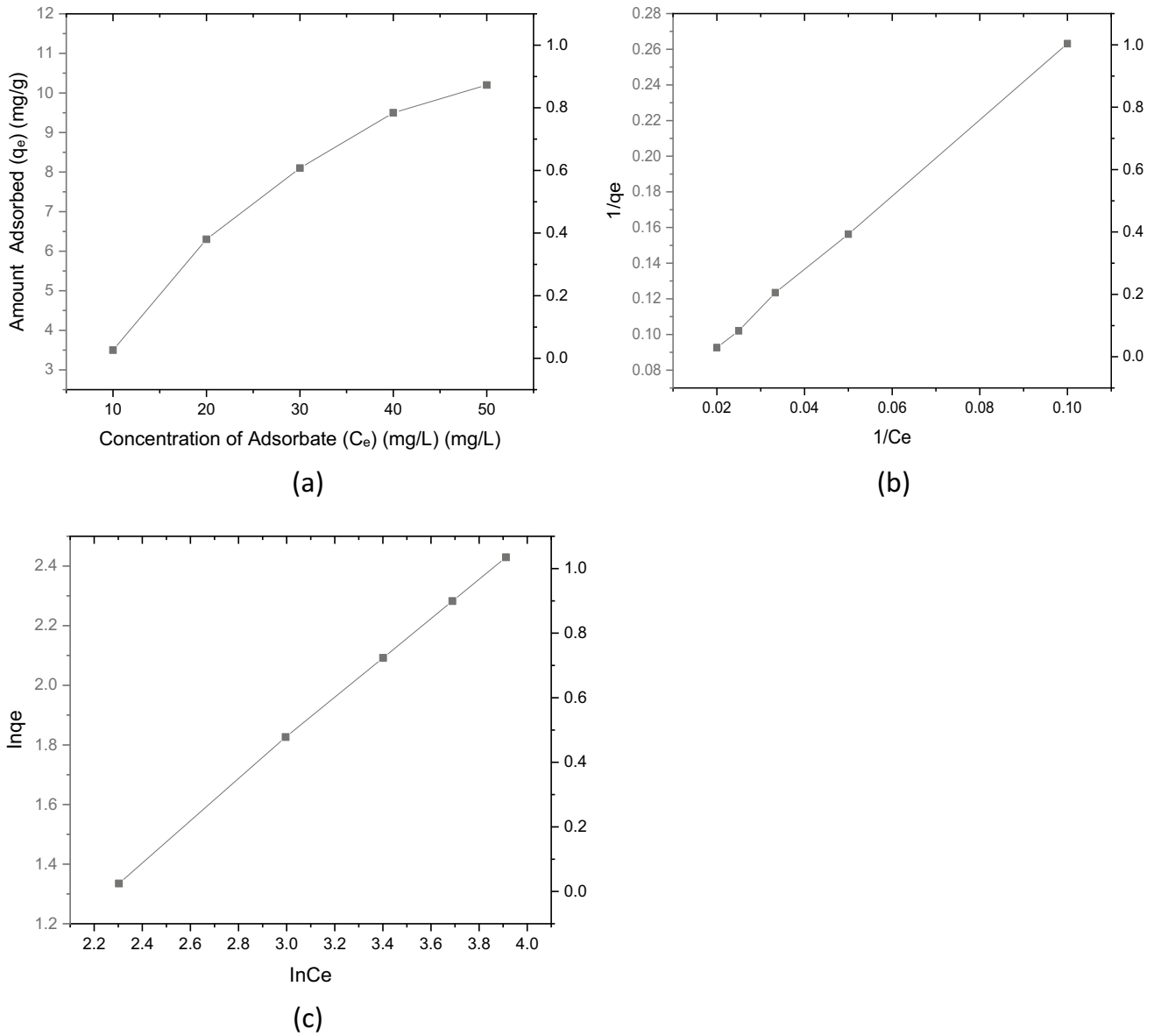

Fig. 5 Adsorption isotherm studies: **a** a graph qe Vs Ce, **b** Langmuir isotherm model (1/qe vs 1/Ce) and **c** Freudrich Isothem model (lnqe vs lnCe)

Table 1 Calculated isotherm parameters of the nanocomposite

Langmuir model		Freundlich model	
q_m(mg/g)	22.98	n	1.529
k_L(L/mg)	0.0184	R^2	0.9996
R^2	0.9944	K_f mg/g	0.823

A plot of $\frac{1}{q_e}$ against $\frac{1}{C_e}$ (Fig. 5b) gave a straight line with a slope of $\frac{1}{K_L q_m}$ and an intercept of $\frac{1}{q_m}$ which was used to determine the constants (K_L and q_m) represented in Table 1. To further understand the adsorption using the Langmuir model, a further characterization was done using a dimensionless parameter, the separation factor R_L [31] using the Eq. (6):

$$R_L = \frac{1}{1 + K_L C_e} \tag{6}$$

where, R_L represents the separation factor, while K_L is the Langmuir equilibrium constant. On the other hand, the Freundlich isotherm is an empirical model used to describe the adsorption of solutes onto a solid surface. It is particularly useful for heterogeneous surfaces and non-ideal adsorption behaviour [15]. The Freundlich isotherm is expressed as in Eq. (7):

$$q_e = K_f C_e^{\frac{1}{n}} \tag{7}$$

In this case, q_e is the amount of adsorbate adsorbed at equilibrium (mg/g or mol/g), C_e is the equilibrium concentration of the adsorbate in the solution (mg/L or mol/L), K_f is the Freundlich constant, related to the adsorption capacity of the adsorbent (mg/g or mol/g), while "n" is the Freundlich exponent, related to the intensity of adsorption which reflects the heterogeneity of the adsorption sites. The equation can be rearranged to form Eq. (8) which was used to plot graph shown in Fig. 5c:

$$Inq_e = \frac{1}{n} InC_e + InK_f \tag{8}$$

Figure 5a show shows a positive trend, where the adsorbed amount (q_e) increases with the equilibrium concentration (C_e). This is a typical behavior in adsorption, where the amount of adsorbate on the adsorbent increases with increasing adsorbate concentration, as more molecules become available for adsorption on the surface. The increase in the amount adsorbed is not linear, suggesting the presence of saturation in the adsorption process. This means the adsorbent's surface is becoming increasingly occupied with adsorbate molecules as the concentration rises. If this trend continues, we would expect that at higher concentrations (beyond the provided data), the rate of increase in adsorption would slow down and eventually plateau as all available adsorption sites are occupied. The maximum adsorption capacity (q_e) seems to be approaching a limit as the concentration increases. The values from the data are increasing at a decreasing rate: from 3.5 mg/g to 6.3 mg/g (increase of 2.8 mg/g), from 6.3 mg/g to 8.1 mg/g (increase of 1.8 mg/g), from 8.1 mg/g to 9.8 mg/g (increase of 1.7 mg/g) and from 9.8 mg/g to 11.3 mg/g (increase of 1.5 mg/g). This suggests that the adsorption rate is slowing down, which could indicate that the adsorbent surface is becoming more saturated, and fewer sites are available for adsorption at higher concentrations.

The adsorption data has been fitted to both the Langmuir (Fig. 5b) and Freundlich isotherm models (Fig. 5c), and the results are shown in the plot. The Langmuir model suggests monolayer adsorption on a uniform surface, with a maximum adsorption capacity of 22.98 mg/g. The Freundlich model accounts for adsorption on a heterogeneous surface, with a heterogeneity factor (n) greater than 1 (Table 1), indicating favourable adsorption. From the plot, both models fit the data. However, a detailed statistical evaluation R^2 show that the Freundlich model provides a better fit to the data compared to the Langmuir model, as indicated by its higher R^2 value. This suggests that the adsorption behaviour is closer to monolayer adsorption on a uniform surface.

4 Conclusion

This paper presents this study has demonstrated so clearly the ability of ethyl ammonium cation to intercalate silicate layers in a polymer matrix. Developing a polycondensed silicate with a polymeric structure was pretty interesting, even when placed in a chitosan polymer matrix. A double-layered structure provides evidence for a proper liking between the chitosan functional groups and the silanol. Surprisingly, the density of the silica particles in the chitosan polymer

matrix has a tremendous effect on the adsorption of Cu^{2+}. This has been proven through the use of different chitosan-silica ratios with 98% of Cu^{2+} removed from model water at an extended pH range of 4 to 6. Based on this reasoning, we have suggested the best chitosan-silica ratio for removing heavy metal Cu^{2+} from contaminated water. Nevertheless, much more research is required on the optimization of the structure of the nanocomposite to understand the interaction between the chitosan functional groups, polycondesed silica and the intercalating agent, ethyl ammonium. Lastly, it is worth mentioning a possible commercial application of this novel material in the treatment and purification of water from areas contaminated by heavy metals. Both chitosan and silica are relatively low-cost raw materials; chitosan, being derived from seafood waste, has an additional sustainability advantage. The chitosan-silica system aligns well with the demand for sustainable materials. Chitosan is biodegradable, and silica is environmentally benign. However, silica precursors (like TEOS) may be expensive. Using cheaper alternatives (e.g., sodium silicate) can reduce production costs. The intercalation system method for chitosan-silica nanocomposites is technically scalable but requires process optimization and cost reduction to become commercially viable for water treatment.

Acknowledgements The authors are grateful for the support from the University of Dodoma, Nelson Mandela African Institution of Science and Technology and the Department of Fusion and Chemical Engineering, Hanyang University, South Korea. Additionally, we would like to express our gratitude to Dr. Godlisten Namwel Shao for sharing his expertise.

Author contributions I.O: Conceptualization, Methodology, Writing an original draft, Data curation. A.H: Writing- Reviewing and Editing.

Data availability All data generated or analyzed during this study are included in this published article and its supplementary information files.

Declarations

Competing interests The authors declare no competing interests.

References

1. Li YH, et al. Removal of Cu^{2+} ions from aqueous solutions by carbon nanotubes. Adsorpt Sci Technol. 2003;21(5):475–86. https://doi.org/10.1260/026361703769645807.
2. Banivaheb S, Dan S, Hashemipour H, Kalantari M. Synthesis of modified chitosan TiO_2 and SiO_2 hydrogel nanocomposites for cadmium removal. J Saudi Chem Soc. 2021. https://doi.org/10.1016/j.jscs.2021.101283.
3. Dan S, Kalantari M, Kamyabi A, et al. Synthesis of chitosan-g-itaconic acid hydrogel as an antibacterial drug carrier: optimization through RSM-CCD. Polym Bull. 2022;79:8575–98. https://doi.org/10.1007/s00289-021-03903-7.
4. Dan S, Banivaheb S, Hashemipour H, Kalantari M. Synthesis, characterization and absorption study of chitosan-g-poly(acrylamide-co-itaconic acid) hydrogel. Polym Bull. 2021;78(4):1887–907. https://doi.org/10.1007/s00289-020-03190-8.
5. Aranaz I, et al. Functional characterization of chitin and chitosan. Curr Chem Biol. 2012;3(2):203–30. https://doi.org/10.2174/2212796810903020203.
6. Desai K, Kit K, Li J, Michael Davidson P, Zivanovic S, Meyer H. Nanofibrous chitosan non-wovens for filtration applications. Polymer. 2009;50(15):3661–9. https://doi.org/10.1016/j.polymer.2009.05.058.
7. Lai SM, Yang AJM, Chen WC, Hsiao JF. The properties and preparation of chitosan/silica hybrids using sol-gel process. Polym - Plast Technol Eng. 2006;45(9):997–1003. https://doi.org/10.1080/03602550600726269.
8. Shetty AR. Metal anion removal from wastewater using chitosan in a polymer enhanced diafiltration system. 2006. pp. 1–86.
9. Liu YL, Hsu CY, Su YH, Lai JY. Chitosan-silica complex membranes from sulfonic acid functionalized silica nanoparticles for pervaporation dehydration of ethanol-water solutions. Biomacromol. 2005;6(1):368–73. https://doi.org/10.1021/bm049531w.
10. Rinaudo M. Chitin and chitosan: properties and applications. Prog Polym Sci. 2006;31(7):603–32. https://doi.org/10.1016/j.progpolymsci.2006.06.001.
11. Giannelis EP. Polymer layered silicate nanocomposites. Adv Mater. 1996;8(1):29–35. https://doi.org/10.1002/adma.19960080104.
12. Jongwattanapisan P, et al. In vitro study of the SBF and osteoblast-like cells on hydroxyapatite/chitosan-silica nanocomposite. Mater Sci Eng C. 2011;31(2):290–9. https://doi.org/10.1016/j.msec.2010.09.009.
13. Huang H, Yuan Q, Yang X. Morphology study of gold-chitosan nanocomposites. J Colloid Interface Sci. 2005;282(1):26–31. https://doi.org/10.1016/j.jcis.2004.08.063.

14. Aguado J, Arsuaga JM, Arencibia A, Lindo M, Gascón V. Aqueous heavy metals removal by adsorption on amine-functionalized mesoporous silica. J Hazard Mater. 2009;163(1):213–21. https://doi.org/10.1016/j.jhazmat.2008.06.080.
15. Chen AH, Liu SC, Chen CY, Chen CY. Comparative adsorption of Cu(II), Zn(II), and Pb(II) ions in aqueous solution on the crosslinked chitosan with epichlorohydrin. J Hazard Mater. 2008;154(1–3):184–91. https://doi.org/10.1016/j.jhazmat.2007.10.009.
16. Kickelbick G. Concepts for the incorporation of inorganic building blocks into organic polymers on a nanoscale. Prog Polym Sci. 2003;28(1):83.
17. Falahati M, Ma'Mani L, Saboury AA, Shafiee A, Foroumadi A, Badiei AR. Aminopropyl-functionalized cubic Ia3d mesoporous silica nanoparticle as an efficient support for immobilization of superoxide dismutase. Biochim Biophys Acta Proteins Proteom. 2011;1814(9):1195–202. https://doi.org/10.1016/j.bbapap.2011.04.005.
18. Yuan Y, Chesnutt BM, Haggard WO, Bumgardner JD. Deacetylation of chitosan: material characterization and in vitro evaluation via albumin adsorption and pre-osteoblastic cell cultures. Materials. 2011;4(8):1399–416. https://doi.org/10.3390/ma4081399.
19. Silva GS, Oliveira PC, Giordani DS, De Castro HF. Chitosan/siloxane hybrid polymer: synthesis, characterization and performance as a support for immobilizing enzyme. J Braz Chem Soc. 2011;22(8):1407–17. https://doi.org/10.1590/S0103-50532011000800003.
20. Brugnerotto J, Lizardi J, Goycoolea FM, Argüelles-Monal W, Desbrières J, Rinaudo M. An infrared investigation in relation with chitin and chitosan characterization. Polymer. 2001;42(8):3569–80. https://doi.org/10.1016/S0032-3861(00)00713-8.
21. Kumirska J, et al. Application of spectroscopic methods for structural analysis of chitin and chitosan. Mar Drugs. 2010;8(5):1567–636. https://doi.org/10.3390/md8051567.
22. Kunjachan S, Jose S. Understanding the mechanism of ionic gelation for synthesis of chitosan nanoparticles using qualitative techniques. Asian J Pharm. 2010;4(2):148–53. https://doi.org/10.4103/0973-8398.68467.
23. Delaila Tumin N, Chuah AL, Zawani Z, Rashid SA. Adsorption of copper from aqueous solution by Elais Guineensis kernel activated carbon. J Eng Sci Technol. 2008;3(2):180–9.
24. Özacar M, Şengil IA. Adsorption of metal complex dyes from aqueous solutions by pine sawdust. Bioresour Technol. 2005;96(7):791–5. https://doi.org/10.1016/j.biortech.2004.07.011.
25. Juang RS, Shao HJ. Effect of pH on competitive adsorption of Cu(II), Ni(II), and Zn(II) from water onto chitosan beads. Adsorption. 2002;8(1):71–8. https://doi.org/10.1023/A:1015222607996.
26. Davis JA, Leckie JO. Effect of adsorbed complexing ligands on trace metal uptake by hydrous oxides. Environ Sci Technol. 1978;12(12):1309–15. https://doi.org/10.1021/es60147a006.
27. Li N, Bai R. Copper adsorption on chitosan-cellulose hydrogel beads: behaviors and mechanisms. Sep Purif Technol. 2005;42(3):237–47. https://doi.org/10.1016/j.seppur.2004.08.002.
28. Aydin H, Yerlikaya Ç, Uzan S. Equilibrium and kinetic studies of copper (II) ion uptake by modified wheat shells. Desalin Water Treat. 2012;44(1–3):296–305. https://doi.org/10.1080/19443994.2012.691745.
29. Lombardo SJ, Bell AT. A review of theoretical models of adsorption, diffusion, desorption, and reaction of gases on metal surfaces. Surf Sci Rep. 1991;13(1–2):3–72. https://doi.org/10.1016/0167-5729(91)90004-H.
30. Piron E, Domard A. Interaction between chitosan and uranyl ions. Part 1. Role of physicochemical parameters. Int J Biol Macromol. 1997;21(4):327–35. https://doi.org/10.1016/S0141-8130(97)00081-0.
31. Hosseinkhani O, Hamzehlouy A, Dan S, Sanchouli N, Tavakkoli M, Hashemipour H. Graphene oxide/ZnO nanocomposites for efficient removal of heavy metal and organic contaminants from water. Arab J Chem. 2023;16(10):105176. https://doi.org/10.1016/j.arabjc.2023.105176.